HIPPOCAMPUS 13:728–744 (2003)

Electrophysiological and Morphological Diversity of Neurons From the Rat Subicular Complex In Vitro

L. Menendez de la Prida,* F. Suarez, and M.A. Pozo

Brain Mapping Unit, Instituto Pluridisciplinar, Universidad Complutense de Madrid, Madrid, Spain

ABSTRACT: We combined whole-cell recordings with Neurobiotin labeling to examine the electrophysiological and morphological properties of neurons from the ventral subicular complex in vitro (including the subicular, presubicular, and parasubicular areas). No a priori morphological sampling criteria were used to select cells. Cells were classified as bursting (IB), regular-spiking (RS), and fast-spiking (FS) according to their firing patterns in response to depolarizing current pulses. A number of cells remained unclassified. We found 54% RS, 26% IB, 11% FS, and 9% unclassified cells out of a total of 131 neurons examined. We also found cells showing intrinsic membrane potential oscillations (MPO) (6%), which represented a subgroup of the unclassified cells. We analyzed several electrophysiological parameters and found that RS and IB cells can be subclassified into two separate subgroups. RS cells were subclassified as tonic and adapting, according to the degree of firing adaptation. Both responded with single spikes to orthodromic stimulation. IB cells were subclassified in two subgroups according to their capacity to fire more than one burst, and showed different responses to orthodromic stimulation. We observed that bursting in these two subgroups appeared to involve both Ca^{2+} and persistent Na^{+} components. Both IB and RS cells, as well as MPO neurons, were projecting cells. FS cells were morphologically identified as local circuit interneurons. We also analyzed the spatial distribution of these cell types from the vicinity of CA1 to the parasubicular areas. We conclude that, in contrast to the commonly accepted idea of the subicular complex as a bursting structure, there is a wide electrophysiological variability even within a given cellular group.

KEY WORDS: subiculum; morphology; electrophysiology; Neurobiotin; hippocampus

INTRODUCTION

The subicular complex comprises the subicular, presubicular (PrS), and parasubicular (PaS) areas, and constitutes the anatomical transition zone between the hippocampus and the entorhinal cortex (Köhler, 1986a, b; Van Groen and Lopes da Silva, 1986; Witter, 1993; Naber and Witter, 1998). The subicular complex is involved in the pathophysiology of mental disorders such as Alzheimer's disease (Davies et al., 1988; Flood, 1991) and schizophrenia (Gray et al., 1991), and is a potential site for the action of antipsychotic drugs (Greene, 1996). Because of its strategic position in controlling input and output activity from the hippocampal formation, a role has also been proposed for the subicular complex in temporal lobe epilepsy (Behr and Heinemann, 1996; Harris and Stewart, 2001). Functionally, the subicular complex is involved in spatial encoding through the activity of place cells that respond as a function of the animal's head direction (Taube et al., 1990; Sharp and Green, 1994).

The electrophysiological properties of neurons from the subiculum have been the subject of study, with cells being classified according to their firing properties as bursting or nonbursting both in vivo (Finch et al, 1988; Sharp and Green, 1994; Gigg et al., 2000) and in vitro (Stewart and Wong, 1993; Mason, 1993; Mattia et al., 1993; Taube, 1993; Stanford et al., 1998; Staff et al., 2000). While different laboratories agree on this classification scheme, there is debate with regard to the fraction of cells in each category (Greene and Totterdell, 1997; Menendez de la Prida et al., 2002) and their underlying bursting mechanisms. Using sharp electrodes, Taube (1993) found 69% bursting cells and 31% nonbursting regular-spiking cells in slices from Sprague-Dawley rats. This bursting cell fraction is similar to that reported in guinea pigs (Stewart and Wong, 1993) and in Wistar rats (Mason, 1993). However, Behr et al. (1996) found 54%, whereas Mattia et al. (1993) reported 100%. Recently, using whole-cell recordings in 2–9-week old rats, Staff et al. (2000) found that 68% of those visually selected pyramidal cells were of the bursting type.

Morphologically, various samples of subicular cells loaded with dye have been investigated. Taube (1993) examined the anatomy of four bursting cells and one regular-spiking cell, observing no morphological difference. Seven bursting cells and one regular-spiking cell were stained by Mason (1993), but their anatomy was not analyzed in detail. A more exhaustive anatomical study was performed by Greene and Totterdell (1997) on 30 cells, of which 18 were bursting and 12 nonbursting. Their results suggest that bursting neurons have pyramidal morphology, whereas nonbursting neurons have ei-

Grant sponsor: Comunidad Autónoma de Madrid; Grant numbers: 08.5/0023.3/99; 08.5/0072/2000; Grant sponsor: Ministerio de Ciencia y Tecnología; Grant number: SAF2000-0140.
*Correspondence to: Menendez de la Prida, Brain Mapping Unit, Instituto Pluridisciplinar, Universidad Complutense de Madrid, Paseo Juan XXIII, 1, Madrid 28040, Spain. E-mail: liset.m.prida@hrc.es
Accepted for publication 17 September 2002
DOI 10.1002/hipo.10123

ther pyramidal or nonpyramidal morphology. In two recent studies, the morphological properties of apical and basal dendrites of subicular principal cells were examined in detail (Staff et al., 2000; Harris et al., 2001). No clear correlation was found between the dendritic patterns and the electrophysiological phenotypes.

One of the most controversial results obtained from different laboratories is related to the ionic mechanisms underlying bursting. Some investigators have suggested that Ca^{2+} currents are responsible for bursting, since tetrodotoxin (TTX)-resistant spikes and humps were present in voltage traces from bursting neurons (Stewart and Wong, 1993; Taube, 1993). In contrast, Mattia et al. (1993, 1997) did not find TTX-resistant spikes and suggested that a voltage-dependent Na^+ conductance underlies bursting. A recent detailed study suggested an alternative hypothesis (Jung et al., 2001). By combining patch-clamp recordings and Ca^{2+} imaging, these authors proposed that a tail current drives bursting in these cells. Although they do not rule out a possible Na^+ contribution, their pharmacological results suggest a Ca^{2+} origin. More interestingly, they described two subpopulations of bursting cells, i.e., strong bursting and weak bursting cells, that show different amounts of Ca^{2+} tail currents (Staff et al., 2000; Jung et al., 2001).

Understanding the role of the subicular complex in both normal and pathological situations requires a good knowledge of its electrophysiological and morphological aspects. The large fraction of subicular bursting cells reported by several laboratories has resulted in the assumption that the whole subicular complex behaves as an intrinsically bursting structure. Although bursting may be a key property of many subicular cells, the presence of other electrophysiological phenotypes should not be underestimated, especially if their proportions are not completely clear. Also, little is known about the electrophysiological and morphological properties of cells from the PrS and PaS areas, for which a role in synchronizing activity has been suggested (Behr and Heinemann, 1996; Funahashi et al., 1999; Harris and Stewart, 2001). In the present study, we examined the electrophysiological and morphological properties of cells from the ventral subicular complex. We found that a wide electrophysiological diversity is present and that bursting is not the principal electrophysiological phenotype.

MATERIALS AND METHODS

Preparation of Slices

Experiments were performed in tissue taken from 17–22-day-old Wistar rats. Animal care and use was in accordance with the guidelines approved by the University Complutense of Madrid. Rats were decapitated under ether anesthesia, and the brain was removed and chilled in 4°C oxygenated (95% O_2/5% CO_2) artificial cerebrospinal fluid (ASCF: 125 mM NaCl, 3 mM KCl, 1 mM $MgSO_4$, 1.2 mM NaH_2PO_4, 2 mM $CaCl_2$, 22 mM $NaHCO_3$, 10 mM glucose in distilled water). Horizontal slices (350 μm) were prepared using a Vibratome (TPI Inc). Slices were maintained in ACSF at room temperature for at least 1 h before being transferred to a submerged type recording chamber (flow rate of 1–1.5 ml/min at 32–34°C) attached to an upright infrared (IR) Olympus DIC microscope.

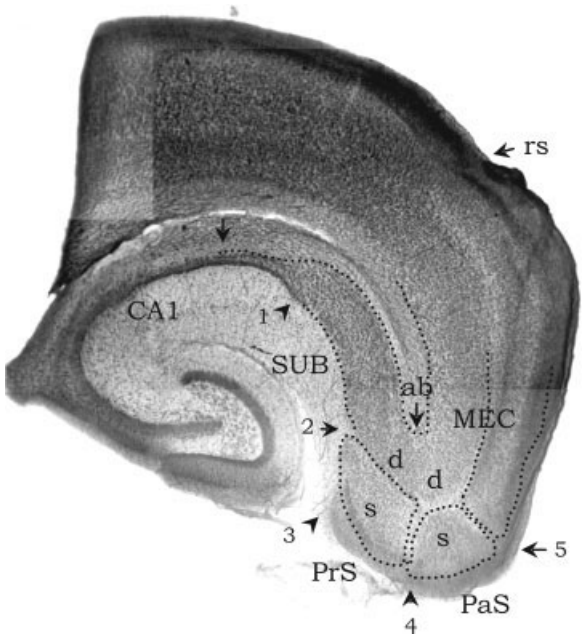

FIGURE 1. Cytoarchitectonic organization of the subicular complex. Photomicrograph of a Nissl-stained horizontal hippocampal/entorhinal cortical slice. Landmarks used to guide recordings are shown. SUB, subiculum; PrS, presubiculum; PaS, parasubiculum; MEC, medial entorhinal cortex; ab, angular bundle; rs, rhinal sulcus; s, superficial layers; d, deep layers.

Electrophysiological Recordings

Somatic whole-cell recordings in current-clamp mode were made using an Axoclamp 2B amplifier (Axon Instruments), digitized (Digidata 1322A; Axon Instruments) and stored on disk at 10-KHz sampling frequency. Patch pipettes were filled with intracellular solution containing (in mM): 131 K-gluconate, 6 KCl, 1 $MgCl_2$, 1 NaCl, 1 EGTA, 5 HEPES, 2 K_2ATP; 0.3 NaGTP, pH 7.3 adjusted with KOH and osmolarity of 290–300 mOsm. For subsequent morphological analysis 0.1–0.5% Neurobiotin (Vector Laboratories, Burlingame, CA) was added to the internal solution. Patch pipettes had a resistance of 4–6 MΩ. Capacitance compensation and bridge balance were carried out.

Recordings were made from the cell layer of the subiculum (SUB) and from both deep (d) and superficial (s) cell layers of PrS and PaS areas. Electrodes were initially placed under visual guidance using a 4× lens. We initially analyzed a series of Nissl-stained sections (n = 17 slices from three rats) to derive landmarks of the SUB, PrS, and PaS areas for visual electrode placement (Fig. 1). SUB cell layer was considered to be from the end of the CA1 stratum-pyramidale layer (arrow 1) to the midlevel of the fascia dentata (arrow 2). Recordings near to these boundaries were avoided. Marks for the PrS were from the midlevel of the fascia dentata (arrow 2) to the outer limit of the hippocampal fissure (arrow 3). Marks for the PaS were at the knee of the transition between the subicular complex and the entorhinal cortex (arrow 5)

and at the midpoint between the outer limit of the hippocampal fissure and the knee point (arrow 4; see also Paxinos and Watson, 1986). Limits of the PrS and PaS areas were also confirmed by looking at the appearance of layer II with a 60× water immersion objective; i.e., PrS layer II has a very compact appearance that changes abruptly to a broad appearance in the PaS, being compact again at the MEC border (Köhler, 1986a, b; Funahashi and Stewart, 1997a, b). Separation line between deep and superficial layers of PrS and PaS was extrapolated from the MEC layer V limit (Fig. 1) (see also Köhler, 1986a) and from radial extensions of superficial layers to the angular bundle (arrow ab). Cell location was drawn in all cases. The cell location of those neurons labeled with Neurobiotin was reexamined.

For whole-cell recordings, a 60× immersion objective was subsequently used. No a priori morphological criterion was adopted to select cells for patching; i.e., we patched the healthy first cell found under visual guidance. Stable whole-cell recordings lasted 10–45 min without a significant loss of cell response quality (determined from resting membrane potential, input resistance and presence of overshooting action potentials). A monopolar tungsten electrode was used to deliver extracellular stimuli (0.1 ms, 0.5–1 mA) to the alveus of CA1, while recordings were made from the subiculum. After the experiment, the patch pipette was carefully withdrawn and Neurobiotin was allowed to diffuse for 15–30 min within the axons and dendrites.

Extracellular Solutions and Drugs

Control experiments were performed in normal ACSF as described above. We also used a number of solutions to manipulate Ca^{2+} currents. The composition of the zero- and reduced-Ca^{2+} (1 mM) solutions was the same as the normal ACSF, except that $MgCl_2$ substituted $CaCl_2$ (equimolar substitution). In the zero-Ca^{2+} solution, 1 mM EGTA was added. To prepare the Cd^{2+} (1 mM) and Co^{2+} (2 mM) solutions, NaH_2PO_4 was omitted in the ACSF to avoid precipitation. $NiCl_2$ (50 μM) and CsCl (5 mM) were added to the ACSF from stock solutions. Tetrodotoxin (TTX; Tocris) was dissolved in the ACSF from stock solutions to reach final concentrations (10–500 nM).

For local application experiments a pressure ejection system (General Valve Corp.) was connected to a patch pipette filled with either ACFS or 30 nM TTX (dissolved in ACSF). Neutral red (1%; Sigma) was used initially to adjust pressure (20 psi) and duration (5 ms) required to perfuse a region of ~50 μm around the soma and at >150 μm into the apical dendrite.

Dye Injection and Histology

Neurons loaded with Neurobiotin were processed for morphological analysis. After the experiment, the slice was fixed overnight in 4% paraformaldehyde phosphate-buffered saline (PBS) (0.1 M, pH 7.4). After H_2O_2 (0.3%) and Triton X-100 (0.6%) pretreatment, the slice was processed by incubation in a 1:100 dilution of ABC Kit (Vector Labs) and by a 0.03% solution of 3,3-diaminobenzidine and 0.005% H_2O_2. The slices were abundantly washed in Tris-buffered saline (TBS) (0.5 M) and were mounted on gelatin-coated glass slides using glycerol (50% in TBS) and Eukitt mounting medium (Fluka). Neurobiotin-labeled cells were drawn using a 40× objective and a Camera Lucida attachment.

Data Measurement and Analysis

Various passive membrane properties were measured. Input resistance was determined from cell responses to current pulses of 500-ms duration (amplitude: ±0.05 nA and ±0.1 nA). The membrane time constant was estimated from the fitting of averaged cell responses to 50-ms and −0.1-nA current pulses (2–3 trials), as previously described (Rall, 1969). Action potential (AP) amplitude was measured from resting membrane potential (RMP) to the AP peak, using short depolarizing pulses (50 ms). AP duration was measured at half-amplitude.

We defined four different measurements of the active membrane properties. The sag index measures the rectification shown by some cells in response to long hyperpolarizing pulses (Fig. 2Aa, open circle). The sag index was defined by calculating

$$(V_{sag} - V_s)/V_{sag}$$

where V_{sag} is the sag voltage deflection and V_s is the stationary voltage deflection measured at the end of the hyperpolarizing pulse. Similarly, we defined the rebound index to quantify the tendency of the membrane potential of some cells to bounce over the RMP after injection of hyperpolarizing pulses (Fig. 2Aa, black circle). The rebound index was defined as

$$(V_{reb} - V_s)/V_{reb}$$

where V_{reb} is the rebound voltage deflection. The larger these indices, the greater the tendency of the cell to undergo sags and rebounds. We also measured the size of the afterhyperpolarization (AHP) and afterdepolarization (ADP) that follow an action potential. The AHP/ADP size was calculated from the voltage difference from the action potential threshold to the maximal level of AHP (negative) or ADP (positive) that follows a spike. Finally, we defined the adaptation index to characterize the firing patterns elicited by 0.1–0.3 nA, 500-ms current pulses in nonbursting cells. The adaptation index was defined as the ratio between the first and last interspike intervals elicited by long pulses (Kawaguchi, 1995; Porter et al., 2001). An adaptation index close to zero implies an adapting firing pattern, whereas an adaptation index close to 1 signifies a tonic firing pattern. Electrophysiological measurements were analyzed in detail in randomly selected subsets of neurons, which represent 74% of the 131 cells recorded.

Different morphological measures were analyzed either from camera lucida drawings or directly from a calibrated grid attached to the microscope (using 10× and 60× objectives). Morphological measurements were performed in those cells successfully loaded with Neurobiotin, which represented 63% of the 131 cells recorded. We measured the soma length and width, together with the thickness of the apical dendritic trunk (at 30 μm from the soma). The distance from the soma to the first apical bifurcation was measured only in those cells that have somata in the deep layers to avoid variability due to their relative positions (Harris et al., 2001). The soma size index was computed as the product of the length and width of the soma. The distance between the soma of

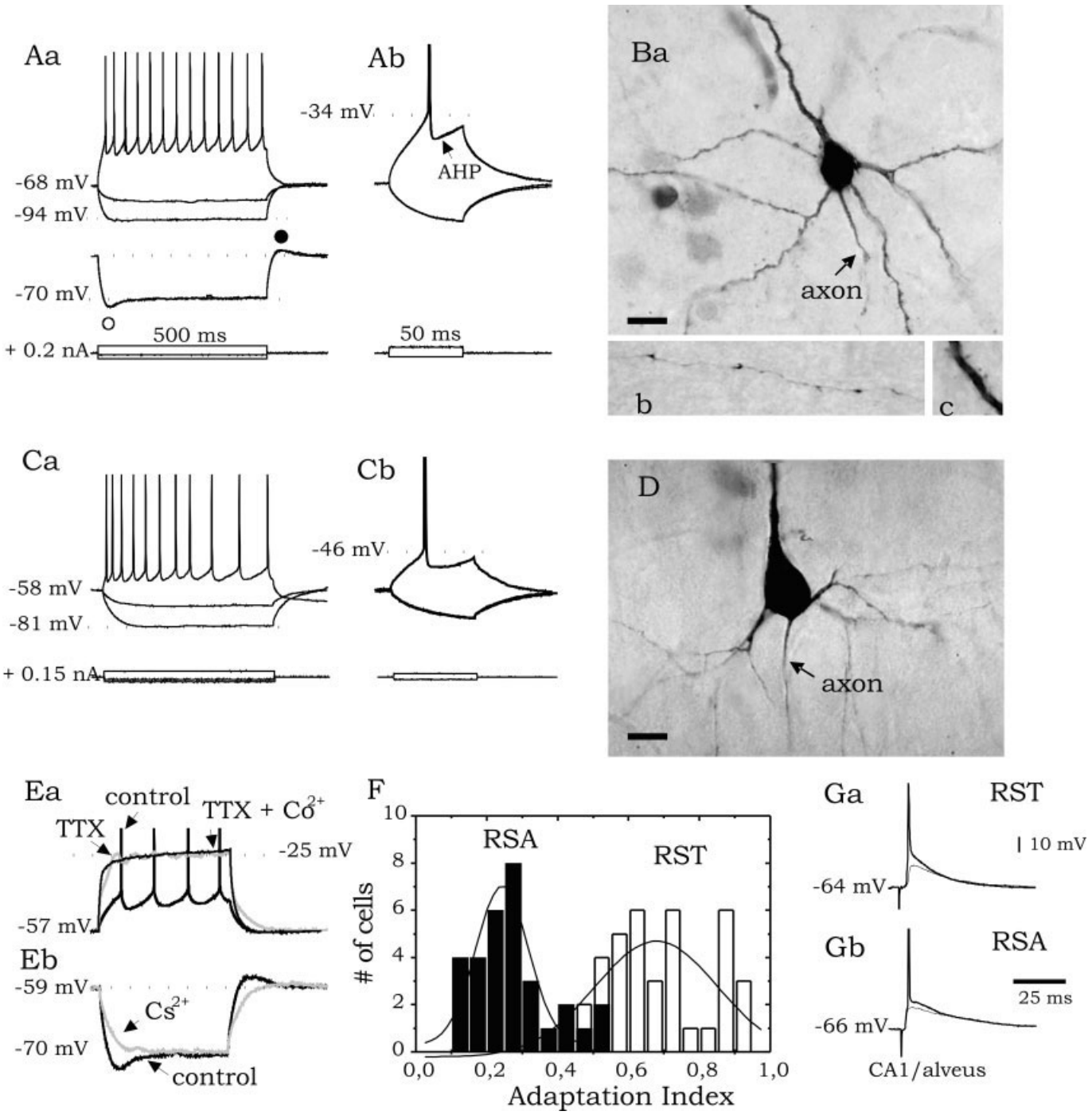

FIGURE 2. Electrophysiological properties of subicular regular-spiking cells. A: Representative electrophysiological responses of regular-spiking tonic (RST) cells to depolarizing and hyperpolarizing current pulses (Aa). Sags (○) and rebounds (●) were rarely observed in these cells (lower voltage trace from a different cell), which typically exhibited afterhyperpolarizations (AHPs) after action potentials (Ab). B: Photomicrograph of the cell whose responses are shown in A loaded with Neurobiotin for morphological analysis (Ba). RST cells were projecting neurons with axon collaterals found in the alveus of CA1 (Bb). Many also had numerous spines (Bc). C: Representative electrophysiological responses of regular-spiking adapting (RSA) cells to depolarizing and hyperpolarizing current pulses (a). RSA cells also exhibited an AHP after individual spikes (b). D: Photomicrograph of an RSA cell. E: Tetrodotoxin (TTX)-resistant humps (Ea) revealed in an RST cell by 200 nM TTX (gray trace, response to 300-ms current pulses). These humps were blocked by 2 mM Co^{2+}. Sags and rebounds (Eb) in regular-spiking cells were blocked by 5 mM Cs^{+} (gray trace). F: Adaptation index distributions from all RSA and RST cells included in this study. The two distributions were statistically different at $P < 0.005$ (Student's *t*-test). G: Orthodromic responses of subicular RST (Ga) and RSA (Gb) cells to alvear stimulation. Scale bars = 12 μm in Ba, 17 μm in Bb, and 13 μm in Bc.

TABLE 1.

*Electrophysiological Properties of Cells**

	RST	RSA	IB$^-$	IB$^+$	FS	MPO
RMP (mV)	−58.7 ± 4.2	−60.7 ± 2.4	−60.3 ± 3.5	−62.3 ± 3.4	−66.2 ± 6.1	−58.2 ± 4.2
Time constant, τ_m (ms)	10.7 ± 3.1	13.6 ± 3.5	9.7 ± 1.8	9.8 ± 1.9	16.6 ± 4.9	15.4 ± 3.2
Input resistance (MΩ)	99 ± 32	154 ± 46	82 ± 31	81 ± 24	204 ± 120	150 ± 81
AP amplitude (mV)	92.7 ± 6.3	88.4 ± 9.1	97.9 ± 6.7	98.1 ± 3.8	90.4 ± 10.1	85.9 ± 4.9
AP duration (ms)	0.89 ± 0.11	0.82 ± 0.15	0.86 ± 0.15	0.94 ± 0.19	0.77 ± 0.11	0.98 ± 0.14
Sag index	0.05 ± 0.03	0.08 ± 0.05	0.13 ± 0.04	0.13 ± 0.03	0.06 ± 0.02	0.08 ± 0.07
Rebound index	0.08 ± 0.04	0.07 ± 0.05	0.12 ± 0.05	0.14 ± 0.06	0.02 ± 0.01	0.04 ± 0.02
AHP/ADP size (mV)	−8.5 ± 5.3	−8.2 ± 3.9	−0.2 ± 2.1	—	−11.2 ± 5.3	−9.9 ± 2.5
Adaptation index	0.72 ± 0.16	0.27 ± 0.11	—	—	0.58 ± 0.23	—
n	25	19	20	14	11	8

RST, regular-spiking tonic; RSA, regular-spiking adapting; IB$^-$, IB$^+$, weak bursting, strong bursting; FS, fast-spiking; MPO, membrane potential oscillations; RMP, resting membrane potential; AP, action potential; AHP/ADP, after hyperpolarization/after depolarization; PrS, presubicular; PaS, parasubicular.

*Data from the subiculum and deep layers of PrS and PaS (see also Table 3).

Neurobiotin-loaded cells and the alveus (or the angular bundle in the case of cells from PrS and PaS) was estimated using the calibrated grid and 4× lens. The presence of spines was examined with the 60× objective. Only those cells with the highest quality of Neurobiotin loading were used to examine the amount of spines (classified as spiny, poorly spiny, and no-spiny). The examination of projecting cells was performed solely in those Neurobiotin-loaded neurons in which numerous axon collaterals were clearly visualized. Cells showing sectioned axons were not considered.

All results are given as mean ±SD, with the number of cells indicated in each case. The results were compared using either Student's *t*-test or analysis of variance (ANOVA). The significance level (*P*) is specified in every case.

RESULTS

The results presented in the present study are from stable whole-cell recordings obtained from 131 neurons from the ventral subicular complex. We recorded from cells from the subiculum (n = 53), PrS (n = 37) and PaS (n = 41). A number of cells (n = 39) were recorded in the CA1 pyramidal region of the hippocampus. Neurons were classified as bursting, regular-spiking, and fast-spiking, on the basis of their response to long current injections at RMP.

Regular-Spiking Cells

Seventy-one cells were classified as regular-spiking. These cell responses to suprathreshold current pulses consisted of regular firing of action potentials (Fig. 2Aa, Ca), irrespective of the membrane potential at which current pulses were injected. In all cases, individual action potentials were followed by a transient AHP (Fig. 2Ab,Cb). In general, sags in response to long hyperpolarizing current injections were not present (Fig. 2Ca), although this rectification was found in a number of cells (12/71; Fig. 2Aa, open circle). Similarly, a rebound of the membrane potential after hyperpolarizing current injections was found in some cases (10/71) and was generally associated with the presence of the sag (Fig. 2Aa, black circle). Both the sag and the rebound were blocked by 5 mM Cs^+, suggesting that they were dependent on inward rectifying currents such as I_h (Fig. 2Eb) (Halliwell and Adams, 1982, Stewart and Wong, 1993). As previously reported (Taube, 1993), we detected TTX-resistant humps that were blocked by 2 mM Co^{2+}, suggesting their Ca^{2+} nature (n = 4; Fig. 2Ea).

Regular-spiking cells were subsequently subclassified as regular-spiking tonic (RST, 40/71) and adapting (RSA, 31/71). RST cells typically fired regularly timed spikes during the depolarizing current pulse (Fig. 2Aa). In contrast, RSA cells showed firing adaptation (Fig. 2Ca). We computed the adaptation index from all these cells and found it to be a good measure for subclassifying their firing pattern (Kawaguchi, 1995). RSA cells had low adaptation indices, which were distributed separately from the high adaptation indices obtained from RST cells ($P < 0.005$, Fig. 2F). We further analyzed several electrophysiological measurements in detail in a subset of RSA and RST cells. RST cells had lower input resistance compared with RSA cells ($P < 0.05$; Table 1). Although cells from the deep layers of the PrS and PaS areas exhibited slightly higher input resistance than cells from the subiculum (see Table 3), the statistical difference between RSA and RST cells were always detected. This difference in the input resistance was not found in regular-spiking cells from the superficial layers of the PrS and PaS (see Table 3). Other electrophysiological properties, such as action potential amplitude and duration, membrane time constant, and active property indices, were similar in RSA and RST cells (Table 1).

We also explored the effect of extracellular stimulation of the CA1 alveus in a number of RST (n = 6) and RSA cells (n = 5)

TABLE 2.

*Morphological Properties of the Different Electrophysiological Classes of Cells**

	RST	RSA	IB$^-$	IB$^+$	FS	MPO
Soma shape						
Pyramidal	14/24	8/16	8/15	9/10	0/11	4/6
Nonpyramidal	10/24	8/16	7/15	1/10	12/11	2/6
Soma size index (μm^2)	328 ± 108	303 ± 79	450 ± 99	404 ± 101	263 ± 108	335 ± 61
Apical dendrite width (μm)	2.6 ± 0.7	1.9 ± 0.8	3.3 ± 0.9	2.4 ± 0.8	—	2.2 ± 1.1
Distance to the first apical bifurcation (μm)	89 ± 40	196 ± 91	131 ± 114	228 ± 133	—	160 ± 128
Spines						
S	9/17	4/10	7/10	7/8	0/10	5/6
PS	3/17	1/10	1/10	0/8	2/10	0/6
NS	5/17	5/10	2/10	1/8	8/10	1/6
n	24	16	15	10	11	6

RST, regular-spiking tonic; RSA, regular-spiking adapting; IB$^-$, IB$^+$, weak bursting, strong bursting; FS, fast-spiking; MPO, membrane potential oscillations; S, spiny; PS, poorly spiny; NS, no-spiny.

*Data from the subiculum and deep layers of PrS and PaS (see also Table 3).

from the subiculum. Alvear stimulation elicited excitatory postsynaptic potentials (EPSPs) that were able to trigger single spikes in both RST (Fig. 2Ga) and RSA cells (Fig. 2Gb). Inhibitory postsynaptic potentials (IPSPs) induced by orthodromic stimulation of these cells were observed in only some cases (5/11; not shown).

Morphologically, RSA and RST cells had pyramidal- and nonpyramidal-shaped somata, indistinctly (Fig. 2Ba, D), as well as numerous apical and basal dendrites and axon collaterals (Fig. 2Bb; see also Fig. 7). These cells were also typically spiny (Fig. 2Bc; Table 2). The width of the principal dendrite appeared to be lower in RSA than in RST cells, although not significantly (Table 2). Similarly, the distance to the first apical dendritic bifurcation seems to be shorter in RST than in RSA cells (Table 2).

Axon collaterals from RST cells were reconstructed successfully in 15 cells. RST cells typically sent axons back to the alveus of CA1 and to the deep layers of the PrS and PaS (see Fig. 7B). Numerous axon collaterals were also local. In some cases (n = 5), axon collaterals from RST cells from the subiculum were found in the superficial layers of the PrS and PaS areas (see Fig. 7B). Most RSA cells have axons sectioned by the slicing procedures. In the few cells in which axon collaterals could be reconstructed (n = 3), their projecting patterns were as described in RST cells.

Bursting Cells

Thirty-four cells were classified as bursting cells. Their principal characteristic was to respond with bursts of two or three spikes to depolarizing current pulses at RMP (Fig. 3Aa, Ca). In most of these cells, bursting failed if cells were depolarized beyond −55 mV. In these cases, regular-spiking was recorded (Fig. 3Ea). All bursting neurons exhibited ADPs after individual spikes (Fig. 3Ab, Ca inset), in contrast to regular-spiking cells (see the AHP/ADP size in bursting and regular-spiking cells, Table 1, significantly different at $P < 0.005$).

Bursting cells were subclassified as weak bursting (IB$^-$, 20/34) and strong bursting (IB$^+$, 14/34). IB$^-$ cells fired only one burst at the beginning of the 500-ms depolarizing current pulses (Fig. 3Aa), whereas IB$^+$ cells fired more than one burst (Fig. 3Ca). Another difference was that bursts in IB$^-$ cells had two to three spikes, with the underlying ADP easily isolated by adjusting the current pulse intensity (Fig. 3Ab). In contrast, the first burst in IB$^+$ cells typically had three or more action potentials, and ADPs could not be isolated (Fig. 3Cb). AHPs after bursting were also more prominent in IB$^+$ cells compared with IB$^-$ cells (Fig. 3Ab, Cb). Passive properties were similar in IB$^-$ and IB$^+$ cells (Table 1). They had similar input resistance and membrane time constant, which were significantly lower in bursting cells than in RSA cells ($P < 0.05$; Table 1), but not significantly lower than in RST cells (Table 1). Bursting cells from the subiculum and from the deep and superficial layers of the PrS and PaS area exhibited similar properties (Table 3).

Both IB$^-$ and IB$^+$ cells had sags and rebounds in response to long hyperpolarizing current pulses (Fig. 3Aa, open and black circles; Table 1). In some of these cells, rebounds could activate intrinsic bursts if the membrane was slightly depolarized (Fig. 3Ca, lower trace). The application of 5 mM Cs^+ blocked sags, whereas it only reduced rebounds (n = 5; Fig. 3Eb). These Cs^+-resistant rebounds were more typically present in IB$^+$ cells. They were subsequently eliminated by 50 μM Ni^{2+}, which blocks low-threshold Ca^{2+} currents (n = 5; Fig. 3Eb).

Orthodromic stimulation of bursting cells from the subiculum elicited EPSPs that were able to trigger bursts in IB$^+$ (n = 5; Fig. 3Gb). However, orthodromically activated bursts were found in only one of seven IB$^-$ cells (Fig. 3Ga). No differences in the resting membrane potential accounted for this result. As in regular-spiking cells, IPSPs induced by alvear stimulation were observed in some cases (4/11).

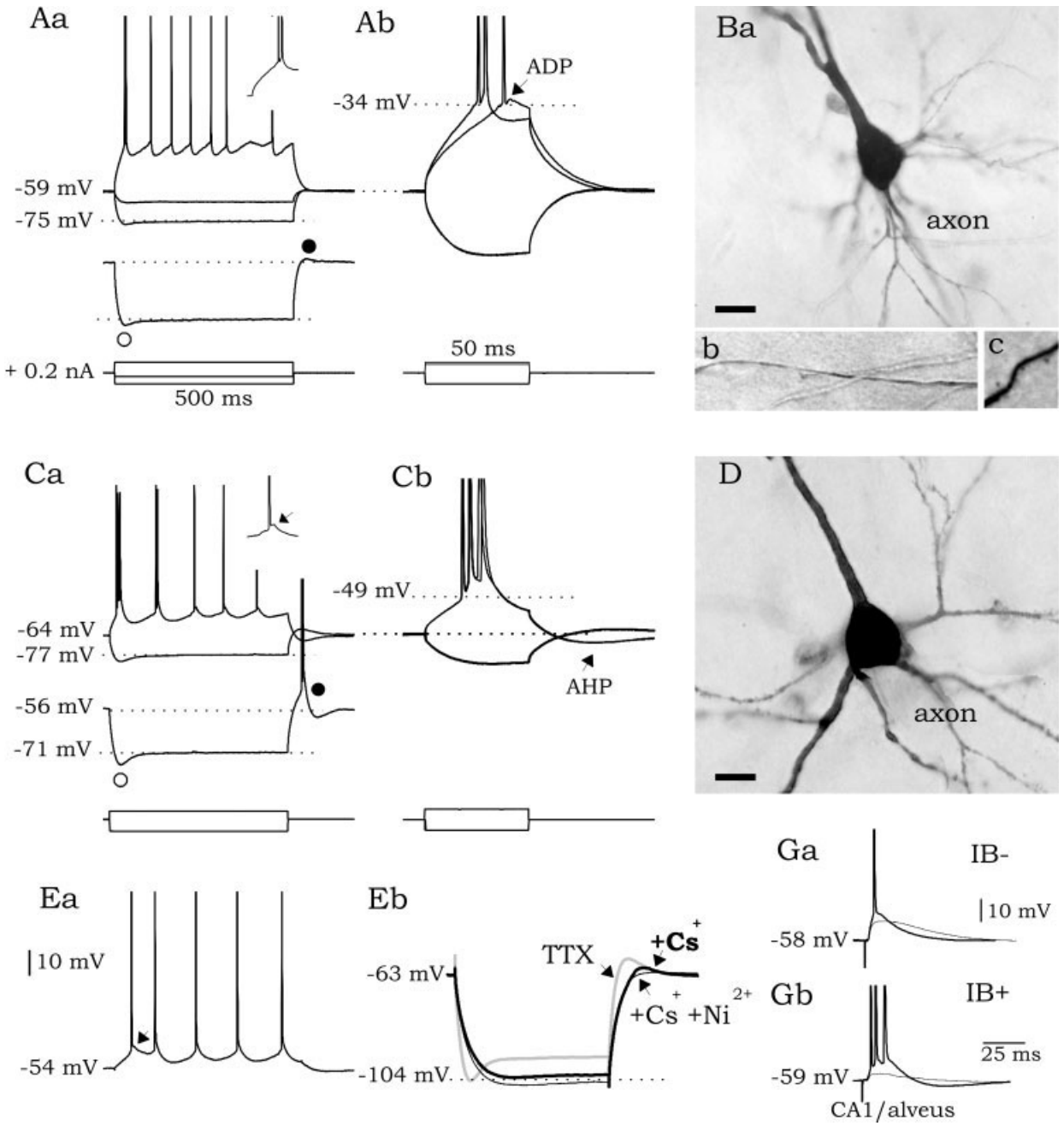

FIGURE 3. Electrophysiological properties of subicular bursting cells. A: Representative electrophysiological responses of weak bursting (IB^-) cells to depolarizing and hyperpolarizing current pulses (Aa). IB^- cells fired only one burst at the beginning of the depolarizing pulse (see inset). Sags (○) and rebounds (●) were typically observed (lower voltage traces). IB^- cells exhibited an afterdepolarization (ADP) after action potentials that were easily revealed by adjusting the intensity of 50-ms current pulses (Ab, same cell than in Aa). B: Photomicrograph of the cell whose responses are shown in A (Ba). IB^- cells were projecting cells (Bb) and had numerous spines (Bc). C: Representative electrophysiological responses of strong bursting (IB^+) cells. IB^+ cells fired more than one burst in response to depolarizing current pulses at resting membrane potential (RMP) (Ca). As in IB^- cells, sags (○) and rebounds (●) were typically reported (lower voltage trace). Rebounds used to activate bursting in some of these cells. In contrast to the case of IB^- cells, adjusting the intensity of 50-ms current pulses did not reveal ADPs in IB^+ cells (Cb). ADPs in IB^+ cells were more evident in the single spikes elicited by long pulses (inset in Ca). D: Photomicrograph of an IB^+ cell. Like IB^- cells, IB^+ cells were also projecting cells. E: (Ea) Bursting in IB^+ and IB^- cells failed if they were depolarized (response from an IB^+ is shown). (Eb) 5 mM Cs^+ blocked sags, but not rebounds (thick black trace). The Cs^+-resistant rebounds were blocked by 50 μM Ni^{2+} (thin black trace). G: Orthodromic responses of subicular IB^- (Ga) and IB^+ (Gb) cells to alvear stimulation. Scale bars = 15 μm in Ba and D, 17 μm in Bb, and 12 μm in Bc.

TABLE 3.

Comparison of Some Electrophysiological and Morphological Properties of Cells Between Areas

	RST	RSA	IB^-	IB^+	FS	MPO
			Subiculum			
RMP (mV)	59.2 ± 3.9 (7)	62.8 ± 3.8 (6)	60.5 ± 2.1 (7)	60.6 ± 4.8 (6)	65.7 ± 7.6 (4)	62.5 ± 2.4 (2)
Time constant, τ_m (ms)	10.3 ± 2.9 (7)	12.6 ± 3.1 (6)	9.1 ± 1.1 (7)	10.5 ± 1.7 (6)	16.7 ± 2.8 (4)	14.6 ± 4.9 (2)
Input resistance (MΩ)	81 ± 33 (7)	146 ± 30 (6)	62 ± 18 (7)	70 ± 16 (6)	275 ± 17 (4)	154 ± 68 (2)
Soma size index (μm^2)	374 ± 22 (7)	364 ± 58 (5)	420 ± 49 (6)	421 ± 91 (5)	283 ± 74 (4)	344 ± 37 (2)
			Pre-subiculum deep			
RMP (mV)	60.8 ± 1.9 (4)	62.8 ± 0.9 (5)	63.4 ± 2.9 (5)	63.1 ± 3.1 (3)	67.7 ± 3.9 (3)	62.1 ± 3.1 (2)
Time constant, τ_m (ms)	11.3 ± 2.4 (4)	11.3 ± 0.4 (5)	10.4 ± 2.1 (5)	9.2 ± 1.9 (3)	14.9 ± 2.6 (3)	15.7 ± 2.6 (2)
Input resistance (Mω)	110 ± 12 (4)	135 ± 53 (5)	94 ± 42 (5)	79 ± 27 (3)	120 ± 35 (3)	208 ± 17 (2)
Soma size index (μm^2)	340 ± 76 (4)	320 ± 71 (3)	323 ± 11 (4)	441 ± 97 (3)	268 ± 31 (3)	308 ± 12 (2)
			Pre-subiculum superficial			
RMP (mV)	70.3 ± 3.1 (5)	67.7 ± 2.5 (4)	—	—	62.1 ± 4.3 (3)	—
Time constant, τ_m (ms)	14.4 ± 1.2 (5)	15.4 ± 1.6 (4)	—	—	12.7 ± 1.7 (3)	—
Input resistance (Mω)	232 ± 51 (5)	205 ± 32 (4)	—	—	291 ± 109 (3)	—
Soma size index (μm^2)	275 ± 73 (4)	180 ± 34 (4)	—	—	225 ± 46 (3)	—
			Para-subiculum deep			
RMP (mV)	65.1 ± 2.9 (4)	64.2 ± 2.2 (5)	67.2 ± 3.1 (4)	69.1 ± 2.1 (3)	69.1 ± 2.6 (4)	66.1 ± 2.7 (4)
Time constant, τ_m (ms)	10.2 ± 2.4 (4)	16.7 ± 1.9 (5)	10.7 ± 1.8 (4)	13.2 ± 2.9 (3)	15.1 ± 1.3 (4)	17.5 ± 1.5 (4)
Input resistance (Mω)	125 ± 14 (4)	190 ± 35 (5)	105 ± 12 (4)	111 ± 18 (3)	176 ± 70 (4)	188 ± 52 (4)
Soma size index (μm^2)	270 ± 77 (4)	282 ± 39 (2)	207 ± 44 (2)	244 ± 65 (2)	198 ± 91 (4)	280 ± 56 (2)
			Para-subiculum superficial			
RMP (mV)	63.6 ± 2.3 (5)	68.6 ± 3.2 (3)	61.3 ± 2.5 (3)	—	68.6 ± 3.8 (3)	—
Time constant, τ_m (ms)	13.3 ± 2.8 (5)	13.9 ± 1.9 (3)	5.7 ± 0.8 (3)	—	15.1 ± 3.2 (3)	—
Input resistance (Mω)	150 ± 65 (5)	190 ± 12 (3)	50 ± 11 (3)	—	194 ± 54 (3)	—
Soma size index (μm^2)	304 ± 79 (5)	229 ± 33 (3)	553 ± 41 (3)	—	246 ± 59 (2)	—

RST, regular-spiking tonic; RSA, regular-spiking adapting; IB^-, IB^+, weak bursting, strong bursting; FS, fast-spiking; MPO, membrane potential oscillations; RMP, resting membrane potential.

Morphologically, the somata of bursting cells were larger than those of regular-spiking cells ($P < 0.05$; Table 2). The most interesting characteristic of IB^+ cells was that most of their somata were pyramid-shaped (9/10), whereas IB^- cells had somata of both pyramidal (8/15) and nonpyramidal oval type (7/15; Table 2). In both cellular subtypes, the distance to the first apical dendritic bifurcation showed considerable variability (coefficient of variation CV = 0.87 and 0.58 in IB^- and IB^+, respectively).

As in regular-spiking cells, most bursting cells had both local and projecting axon collaterals that were successfully reconstructed in 21 cases. Projecting axon collaterals were found in the alveus of CA1 and in both the deep and superficial layers of PrS and PaS (see Fig. 7E–H).

Ionic Mechanisms Underlying Bursting in IB^- and IB^+ Cells

Because of the controversy as to the mechanisms responsible for bursting in subicular neurons, we further explored the ionic basis underlying bursting in both IB^- and IB^+ cells. We aimed to establish whether or not bursting was differently modulated in these subgroups.

We found that bursting in neither IB^+ nor IB^- cells was eliminated by application of blockers of Ca^{2+} currents such as 2 mM Co^{2+} (n = 7), 1 mM Cd^{2+} (n = 5), or zero-Ca^{2+} media (n = 6; Fig. 4Aa,b). However, TTX-resistant spikes and humps were demonstrated in these cells by the application of 200–500 nM TTX (n = 9; Fig. 4Ba,b) at resting membrane potential (no statistical difference was found in the RMP of IB^+ and IB^- cells). TTX-resistant components were still recorded after the application of 5 mM Cs^+ and 50 μM Ni^{2+} (Fig. 4Cb), being subsequently blocked by 2 mM Co^{2+} (Fig. 4Ca,b). Therefore, putative low-threshold and high-threshold Ca^{2+} currents were present in IB^- and IB^+ cells. Interestingly, comparison of the Ca^{2+} contribution elicited by 0.5–0.6 nA depolarizing pulses (quantified as the integral of the subtracted voltage deflections under TTX and TTX +

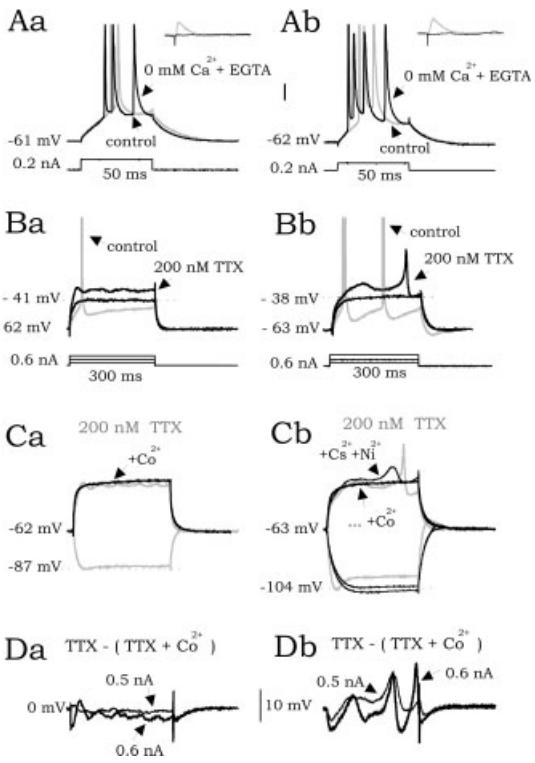

FIGURE 4. Ionic mechanisms underlying bursting in weak bursting (IB^-) and strong bursting (IB) cells, with Ca^{2+} contribution. A: Effect of zero-Ca^{2+} media on bursting elicited in IB^- (Aa) and IB^+ cells (Ab) by 50 ms depolarizing current pulses. Note that under zero-Ca^{2+} media synaptic transmission is blocked (insets). Insets show traces of 120-ms duration. B: Effect of tetrodotoxin (TTX) (200 nM) on IB^- (Ba) and IB^+ cells (Bb). TTX-resistant spikes and humps are recorded in both bursting cell subtypes. C: In both IB^- and IB^+ cells, TTX-resistant spikes and humps (gray traces in Ca and Cb) persist under 5 mM Cs^+ and 50 μM Ni^{2+} (thick black trace in Cb), being blocked by 2 mM Co^{2+} (thin black traces in Ca and Cb). Same cells shown in B; 300-ms pulses. D: Putative Ca^{2+} spikes and humps were estimated in IB^- (Da) and IB^+ cells (Db) by subtracting the voltage deflections elicited under TTX and TTX + Co^{2+} by current pulses of 300-ms duration and 0.5- and 0.6-nA amplitude. Vertical scale bar = 10 mV (5 mV in inset) in A.

Co^{2+}) suggested that IB^+ cells could have larger somatic Ca^{2+} components than IB^- cells: 2.57 ± 0.3 mV · ms and 1.77 ± 0.4 mV · ms for IB^+ and IB^- respectively (Fig. 4Da,b). This is in agreement with previous results that showed larger Ca^{2+} tail currents in IB^+ than in IB^- cells (Jung et al., 2001).

We then examined the contribution of Na^+ currents to ADPs underlying bursting. Because ADPs in IB^+ cells were not easily isolated, we used a reduced Ca^{2+} media (1 mM) to lessen the Ca^{2+} contribution to bursting. Interestingly, reduction of extracellular Ca^{2+} to 1 mM did not significantly affect bursting in IB^- cells (n = 6; Fig. 5Aa), whereas burst duration was reduced in IB^+ cells (n = 6; Fig. 5Ab). Under 1 mM Ca^{2+}, the underlying ADP was easily isolated by adjusting the suprathreshold current pulse intensity in both IB^- and IB^+ cells (Fig. 5Ba,b, left insets). These ADPs were eliminated after 60–70 s of 200 nM TTX application before achieving blockage of Na^+ spikes (Fig. 5Ba,b; see derivatives of the action potentials in the right insets), suggesting a similar contribution of Na^+ components in both bursting types.

However, high concentration of TTX could affect the propagation of action potentials into the dendrites, as well as the back-propagation of dendritic action potentials to the soma (Mackenzie and Murphy, 1998; Magee and Carruth, 1999), thus having the ability to block ADPs by inhibiting putative dendritic contributions. To discriminate this possibility, we examined the effect of low concentrations of TTX (10 nM) on bursting and APDs under

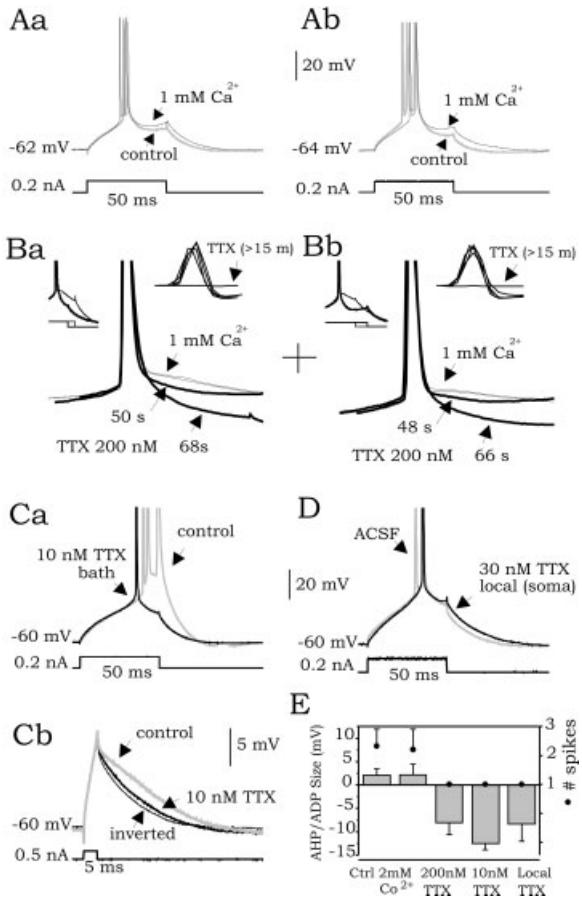

FIGURE 5. Ionic mechanisms underlying bursting in weak bursting (IB^-) and strong bursting (IB^+) cells, with Na^+ contribution. A: Reduction of extracellular Ca^{2+} ($[Ca^{2+}]_o$) to 1 mM decreased burst duration in IB^+ (Ab), but not in IB^- cells (Aa). B: Blocking effect of 200 nM tetrodotoxin (TTX) on ADPs elicited by current pulses of 50 ms in IB^- (Ba) and IB^+ cells under 1 mM $[Ca^{2+}]_o$ (Bb). Insets on left show ADPs before TTX (thick trace) and 68 and 66 s after its application (thin black traces in Ba and Bb, respectively). Insets on right show the derivatives of the action potential before and during TTX application. Derivatives after 15 min of TTX application are indicated. C: Low concentrations of TTX (10 nM) block bursting (Ca) and ADPs elicited by subthreshold current pulses (Cb). D: Effect of somatic application of TTX (30 nM) on bursting. Local application of artificial cerebrospinal fluid (ACSF) do not block bursting, which was eliminated by local application of 30 nM TTX. E: Quantification of the effect of Co^{2+} and TTX on bursting (number of spikes, black dots) and ADPs (afterhyperpolarization/afterdepolarization [AHP]/ADP] size, bars). Vertical scale bar = 10 mV (20 mV in left insets and 30 V/s in right insets); horizontal scale bar = 2.5 ms (30 ms in left insets and 1 ms in right insets) in B.

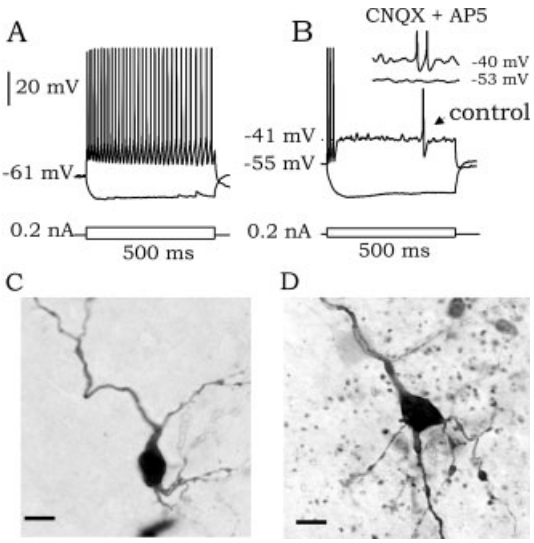

FIGURE 6. Electrophysiological responses of fast-spiking (FS) and membrane potential oscillation (MPO) cells. A: Electrophysiological responses of a typical FS cell to depolarizing and hyperpolarizing current pulses. B: Electrophysiological responses of a typical intrinsic oscillatory MPO cell to depolarizing and hyperpolarizing current pulses. See action potentials interspersed with intrinsic membrane potential oscillations. Inset shows the response of MPO cells under CNQX (10 μM) and AP5 (100 μM) at two different membrane potentials. Spikes are truncated. C: Photomicrograph of the FS cell whose responses are shown in A. D: Photomicrograph of the cell whose responses are shown in B. Scale bars = 15 μm.

normal Ca^{2+} media. We found that bath superfusion of 10 nM TTX eliminated bursting by blocking ADPs in all the cells tested (n = 6; Fig. 5Ca, E). Bursting could not be elicited under these conditions, neither in IB^+ (n = 2) nor in IB^- cells (n = 4), suggesting that Ca^{2+} currents alone were unable to induce it.

We also examined the effect of low concentrations of TTX on the ADPs elicited by subthreshold current pulses, which are not likely to involve dendritic backpropagation of action potentials. ADPs elicited by subthreshold current pulses were detected as membrane potential afterdepolarization (Fig. 5Cb; gray trace elicited by 0.5 nA) that decays back to resting membrane potential more slowly than expected from a passive decay (Fig. 5Cb, inverted trace from −0.5 nA). We found that ADPs elicited by subthreshold current pulses were eliminated by bath superfusion of 10 nM TTX (n = 6; Fig. 5Cb). Finally, we tested the effect of local application of low concentration of TTX (30 nM). In all cases, somatic (n = 5; Fig. 5D) but not dendritic (n = 2; not shown) application of TTX blocked both bursting and ADPs (Fig. 5E).

Fast-Spiking and Unclassified Cells

Fourteen cells were identified as fast-spiking (FS). These cells were characterized by a high rate of action potential firing in response to 500-ms depolarizing current injections (Fig. 6A). FS cells had higher input resistance and membrane time constant than regular-spiking and bursting cells ($P < 0.05$; Table 1). As in regular-spiking cells, sags and rebounds in response to hyperpolarizing current injection were not typically observed (Fig. 6A; Table 1). FS cells showed large AHPs (−11.2 ± 5.3 mV) after single spikes and adaptation indices ranging from 0.33 to 0.96 (n = 11; Table 1). Upon orthodromic stimulation, FS cells from the subiculum responded with EPSPs that were able to trigger single spikes (n = 5; not shown). Anatomical reconstruction of FS cells showed that they were morphologically identified as interneurons (Figs. 6C and 7I,J). They were typically nonpyramidal-shaped and did not have either a clear principal dendritic branch or spines (Table 2). Axonal collaterals of these cells remained locally within the subicular complex (n = 11 cells examined).

Twelve cells remained unclassified, as they did not match any electrophysiological criteria. However, some of these cells shared a similar firing pattern (8/12): in response to depolarizing current pulses, they fired action potentials interspersed with membrane potential oscillations (MPO), similar to those described in cells from the entorhinal cortex (Fig. 6B) (Alonso and Llinas, 1989; Gloveli et al., 2001). The membrane potential oscillations in these cells were independent of synaptic events, as they persisted in the presence of CNQX (10 μM) and AP5 (100 μM) (Fig. 6B, inset). We called these neurons MPO cells. MPO cells had higher input resistance and membrane time constant than RST and bursting cells ($P < 0.05$; Table 1). They did not exhibit sags or rebounds, and a large AHP after single spikes was typically present (Table 1).

Synaptic responses by MPO cells consisted of EPSPs and single spikes (n = 3; not shown). Morphologically, they did not differ from regular-spiking cells, their somata being more of the pyramidal type (4/6; Table 2, Figs. 6D and 7K,L). Axonal collaterals were reconstructed successfully in only two MPO cells with somata in deep PrS layers. These two cells had collaterals in the subiculum and the CA1/alveus direction and in the deep and superficial layers of PrS and PaS.

Spatial Distribution of the Different Cellular Groups

We analyzed the spatial distribution of the different cellular groups throughout the subicular complex. To this purpose, we mapped the position of all recorded cells (n = 170) across the horizontal axis, i.e., from the vicinity of CA1 to the PaS areas (a sample of these cells is shown diagrammatically in Fig. 8A). We found regular-spiking cells to be the most abundant type (Fig. 8B). In the CA1, regular-spiking cells constituted ~80%, whereas they constituted ~ 54% in the subicular complex. This distribution was nearly constant in the subicular, PrS, and PaS areas of the subicular complex (Fig. 8A,B). Bursting cells, constituting ~26%, were more abundant in the subicular and PrS areas, compared with PaS. IB^- cells were more abundant than IB^+ cells (Fig. 8B). MPO cells from the subiculum (~6%) tended to place distally (Fig. 8A), as they were more easily encountered in the PaS area (~15%; Fig. 8B).

To determine the vertical distribution of the different cellular types, we mapped the position of those cells stained with Neurobiotin (n = 78) from the deep to superficial layers of the subicular complex. We first examined the vertical distribution of those cells with their somata in the subicular cell layer and in the deep layers of the PrS and PaS areas (n = 55; Table 4). We did not find

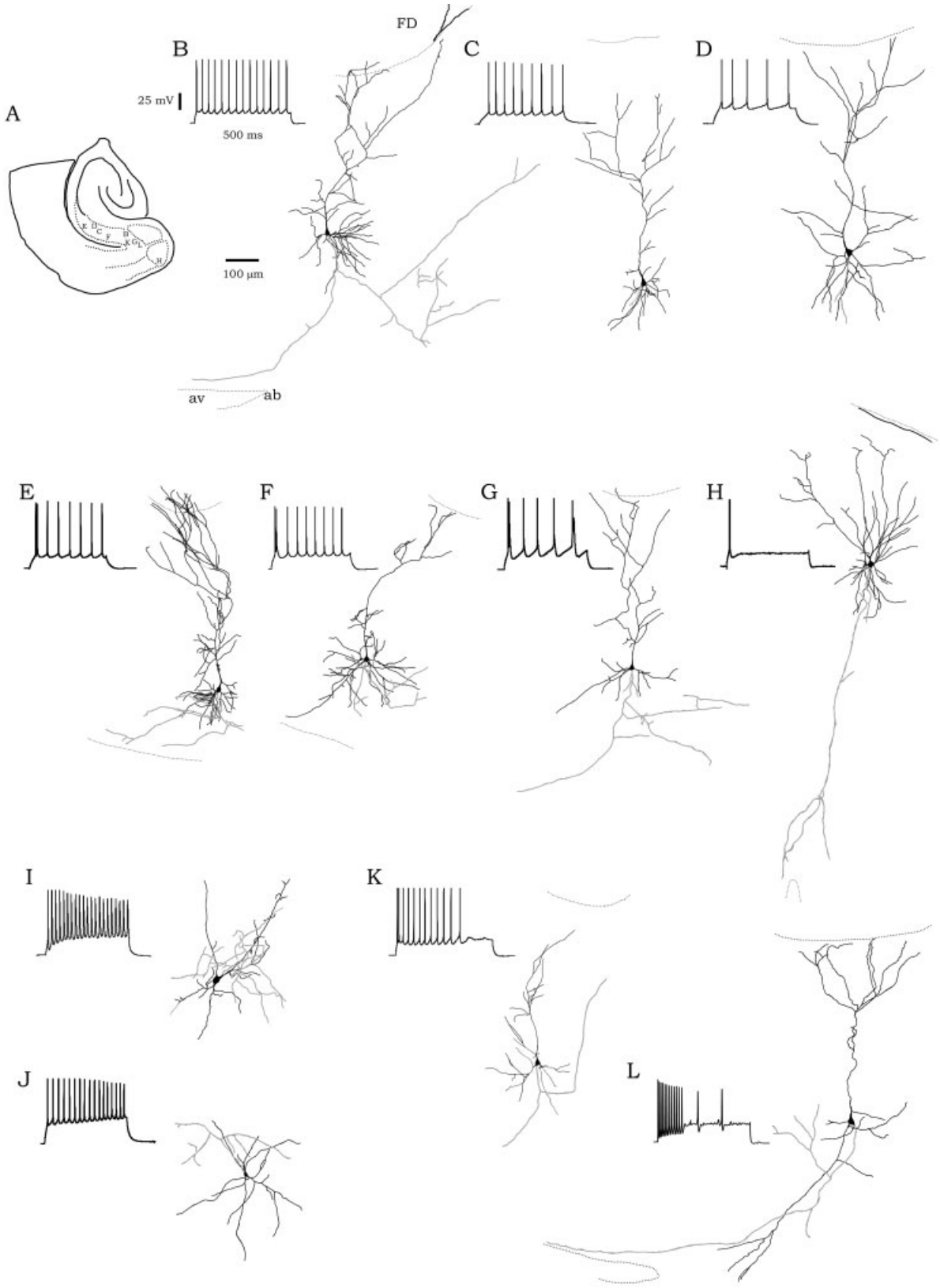

FIGURE 7. Camera lucida drawings of different cells with their corresponding responses to depolarizing current pulses shown at the left. See axon collaterals in gray. Topographic landmarks are shown in discontinuous lines. The slice limit is indicated by a continuous thick line. A: Diagram indicating cell location. B: Drawing of a regular-spiking tonic (RST) cell from the deep presubicular (PrS) layers, with its corresponding response to depolarizing current pulses. C: RST cell (see electric response at the left) from the subiculum. D: Camera lucida drawing of a regular-spiking adapting (RSA) cell recorded from the subiculum. E,F: Drawing of two weak bursting (IB^-) cells recorded from the subiculum. G: Strong bursting (IB^+) cells recorded from the deep layer of the PrS. H: IB^- cells were also recorded in the superficial layers of the parasubicular (PaS). I: Fast-spiking (FS) interneuron from the deep layers of the PrS. See its response to depolarizing current pulses on the left. J: Drawing of an FS interneuron from the deep layers of the PaS. K,L: Drawing of two membrane potential oscillation (MPO) cells recorded from the subiculum (K) and from the deep layers of the PrS (L). FD, fascia dentata; av, alveus; ab, angular bundle.

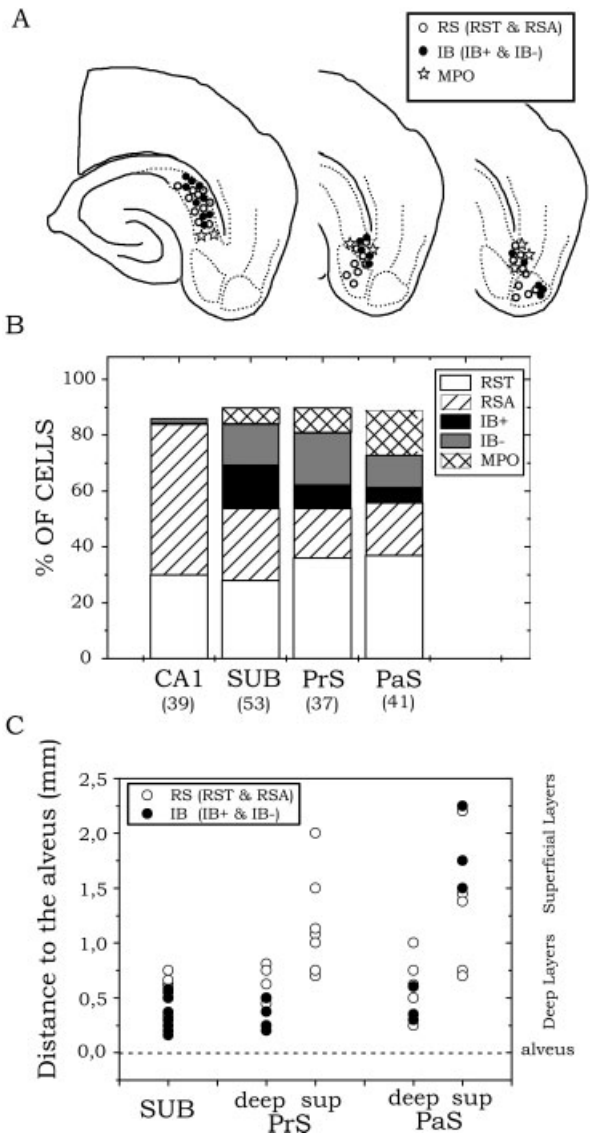

FIGURE 8. Spatial distribution of the different cellular groups. A: Diagram showing the relative cell location of a subset of neurons (n = 56) recorded from the subiculum (left), presubicular (PrS) (middle) and parasubicular (PaS) (right) areas. B: Horizontal distribution of the different electrophysiological types throughout the subicular complex, i.e., from the CA1 to the PaS areas. Fast-spiking (FS) cells are not included (they represent the fraction up to 100% in each area). Membrane potential oscillation (MPO) cells were not recorded in the CA1. C: Vertical distribution of bursting and regular-spiking cells from deep to superficial layers represented as the distance of the somata of Nerobiotin-labeled cells to the alveus.

statistical differences in the distance of these cells to the alveus at a significance level of $P < 0.05$ (Table 4). However, there was a tendency for the bursting cells (especially in the subiculum; Fig. 8C) to be distributed more deeply than regular-spiking cells (Table 4). FS and MPO cells had a random distribution, with FS cells more dispersed (CV = 0.61; Table 4). The vertical distribution of those PrS and PaS cells with their somata located at the superficial layers did not differ particularly between the electrophysiological types (n = 22; Table 4). In the superficial cell layers, bursting cells (IB^-) were only found in the PaS at 1833 ± 381 μm from the alveus (n = 3; see Fig. 7E), similar to regular-spiking cells (1,398 ± 612, n = 15; Figs. 7B and Fig. 8B). Interestingly, MPO cells were not found in the superficial cell layers (Table 4).

DISCUSSION

This work extends the study of the electrophysiological and morphological properties of cells throughout the ventral subicular complex: from the subiculum to PrS and PaS areas. Using no morphological sampling criteria, we found a large variability of cellular types classified according to their response to current injection as bursting, regular-spiking, and fast-spiking cells. We found 54% of regular-spiking neurons, 26% of bursting cells, 11% of fast-spiking interneurons, and 9% of unclassified cells from a total of 131 examined. Interestingly, the unclassified group was mainly composed of cells that showed intrinsic membrane potential oscillations (6%). We also found that both regular-spiking and bursting cells can be subclassified into two separate groups, according to their different electrophysiological criteria.

Spatial Distribution of Subicular Cells

As previously reported in the subiculum, we found a large population of regular-spiking and bursting cells throughout the subicular complex (Stewart and Wong, 1993; Mason, 1993; Mattia et al., 1993; Taube, 1993; Greene and Totterdell, 1997). Taken together, they constitute 80% of the cellular types found in this structure. In contrast to the CA1 area of the hippocampus, where we found 80% regular-spiking cells, the subicular complex was characterized by the presence of bursting cells distributed from the immediate proximity of the CA1 pyramidal area to the PaS regions. Cells from different populations showed different vertical distributions, i.e., from deep to superficial layers, with bursting cells distributed more deeply than regular-spiking cells, especially in the subiculum (Greene and Totterdell, 1997; Harris et al., 2001). Cells characterized by intrinsic membrane potential oscillations were only encountered in the deep layers, whereas fast-spiking interneurons were randomly distributed.

This different spatial distribution of the electrophysiological cell types, from the subiculum to the PrS and PaS areas (Fig. 8A), could help in understanding the function of the subicular complex in terms of its projecting patterns. The efferent organization of the subicular complex was recently analyzed using a slicing procedure that allows the study of sections transverse to the long hippocampal axis (Ishizuka, 2001). Using this preparation, it is shown that subicular cells projecting to the anteroventral thalamic nucleus are located deeper than those projecting to the mammillary nucleus and those projecting to the nucleus accumbens, these last exhibiting the most superficial alignment. According to the arrangement found at the temporal levels (to which our horizontal ventral slices can be suitably compared; see Fig. 8A,C; see also figure 15 in Ishizuka, 2001), bursting cells that tended to exhibit a deeper distribution would be candidates to project to the anteroventral

TABLE 4.

Vertical Distribution of the Different Electrophysiological Classes of Cells

	RST	RSA	IB^-	IB^+	FS	MPO
	Subicular, pre-subicular, and para-subicular deep layers					
Distance to the alveus (μm)	582 ± 180	529 ± 103	472 ± 160	408 ± 169	401 ± 241	508 ± 116
n	15	9	7	11	7	6
	Pre-subicular and para-subicular superficial layers					
Distance to the alveus (μm)	1220 ± 451	1313 ± 416	1833 ± 381	—	1663 ± 440	—
n	9	6	3	0	4	0

RST, resting-spiking tonic; RSA, resting-spiking adapting; IB^-, IB^+, weak bursting, strong bursting; FS, fast-spiking; MPO, membrane potential oscillations.

thalamic nucleus. Similarly, regular-spiking cells, which exhibited an outer distribution, would mainly project to the nucleus accumbens. Nevertheless, bursting and regular-spiking cells were also found in the middle layers, which seem to be the origin of projections to the mammillary nucleus. Interestingly, MPO cells exhibited a clearly distal distribution, which make them candidates for thalamic projections. It would be thus interesting to examine, in the near future, the correlation between the electrophysiological phenotypes and the projecting patterns of the subicular complex.

Electrophysiological Diversity of Subicular Cells

Different laboratories have reported different fractions of bursting cells in the subiculum in vitro, ranging from 54% (Behr et al., 1996) to 100% (Mattia et al., 1993). In vivo recordings have reported a fraction of 57% of bursting cells in the ventral subiculum (16/28; Finch et al., 1988) and of 71% in the dorsal subiculum (5/7; Gigg et al., 2000). Using whole-cell recordings, Staff et al. (2000) reported 68% of bursting cells out of 171 visually selected pyramidal neurons. In the present study, we found a lower fraction of bursting cells, i.e., 30% out of 53 cells recorded in the subiculum, and 26% out of 131 cells recorded throughout the subicular complex. This is, however, a fraction computed from the total number of cells, including interneurons and MPO cells. If we disregard these cellular groups, we found a fraction of 32% of bursting neurons in the subicular complex, which represents 37% of the subiculum.

One possibility that may explain our lower fraction of bursting cells is their different spatial distribution and orientation within the slice. As shown in Figure 8B, bursting cells were found throughout the subicular complex, and were less common in the PaS direction (from 30% to 17% in the proximodistal direction). Also, as shown previously, it may be a different vertical distribution of bursting cells from deep to superficial layers (from ~70% to ~25%; Greene and Totterdell, 1997). Because the subicular complex is prominently folded at the PrS and PaS areas, it is possible that the somatodendritic axis of many subicular cells (especially those from the PrS and PaS deep layers) may be cut by the slicing procedure. This, together with a widespread sampling of cells, could affect the overall proportion of bursting neurons.

However, even in the subiculum, we found a fraction of bursting cells that was lower than previously reported. Previous reports of bursting cell proportion have been described from experiments with sharp electrodes (from 69% to 75%; Taube, 1993; Stewart and Wong, 1993; Mason, 1993; Greene and Totterdell, 1997), although in one case a lower percentage was described (54%; Behr et al., 1996). In our work, bursting cells were found to have larger somata in regular-spiking cells (Table 2), which would make them easier target for blind sharp recordings. Recently, we showed that the fraction of bursting cells in a confined area of the subiculum could vary according to the morphological criteria used during visual-assisted whole-cell recordings (Menendez de la Prida et al., 2002). Using different morphological criteria we found a fraction of bursting neurons that ranged from 30% (no morphological criteria) to 62% (large somata) in rats of 17–22-day-old. Interestingly, we noted a difference in the electrophysiological properties (input resistance, time constant) from those morphologically sampled cells when compared with the original (not morphologically sampled) regular-spiking cells, but not with the original bursting cells (see Fig. 1 and Table 1 in Menendez de la Prida et al., 2002). The input resistance, membrane time constant, and soma size of regular-spiking cells sampled using morphological criteria lie at one tail (statistically different at $P = 0.005$) of the original distribution of regular-spiking cells and within two standard deviations of the original distribution of bursting cells. This finding suggests that by visually selecting larger cells or pyramidal cells in a confined area of the subiculum the bursting will be the predominant cell type and those regular-spiking cells sampled with these criteria will not exhibit difference with bursting cells. It is therefore not likely that the low fraction of bursting cells reported in the present study is related with the age of the rat or with an underestimation of a particular cell type, but with the absence of morphological sampling criteria for cell selection (Menendez de la Prida et al., 2002).

Subicular Bursting Cells

Bursting cells included in this study were subclassified as weak bursting (IB^-) and strong bursting (IB^+), according to the number of bursts elicited by 500-ms depolarizing pulses. Although these cells shared similar passive properties (RMP, input resistance,

and membrane time constant), their synaptic responses were different, with EPSPs able to trigger bursts in IB^+, but not in most IB^- cells. In contrast to previous reports (Funahashi and Stewart, 1997b), we recorded from bursting cells in the PrS and PaS areas. Both IB^+ and IB^- cells typically were found present in the deep layers of the different areas of the subicular complex. Nevertheless, some bursting IB^- cells were encountered in the superficial layers of the PaS. Morphologically, the only difference between these two cell types was that the somata of the IB^+ cells appeared to be of the pyramidal type, whereas IB^- cells had either pyramidal or nonpyramidal morphology, as previously reported (Greene and Totterdell, 1997). Axon collaterals were reconstructed successfully in a number of bursting cells, showing that they project mainly to the CA1/alveus and within the subicular complex.

IB^+ cells were able to generate rhythmic bursting activity upon depolarizing current pulses. Bursts in these cells were also elicited by a rebound from hyperpolarizing potentials. Bursting has been described in several cell types, such as hippocampal, neocortical, and thalamic neurons (Agmon and Connors, 1989; Bal and McCormick, 1993; Traub et al., 1994). Nevertheless, bursting in subicular neurons appears to depend on different ionic mechanisms from those present in other cells.

Previous work has suggested that Ca^{2+} currents are responsible for bursting, since TTX-resistant spikes were recorded in bursting, but not in regular-spiking, neurons (Taube, 1993). Some laboratories have rejected the Ca^{2+} hypothesis in favor of a voltage-dependent Na^+ current hypothesis (Mattia et al., 1993, 1997). Experimental results supporting this idea include the persistence of bursts under blockers of Ca^{2+} currents and their subsequent elimination with TTX. Nevertheless, these two hypotheses are compatible, as Ca^{2+} and Na^+ components can be present concomitantly. The persistence of bursts under blockers of Ca^{2+} currents (Ni^2, Co^{2+}, Cd^{2+}) and with zero-Ca^{2+} media does not exclude a Ca^{2+} contribution, especially if other inward conductances are involved in determining afterdepolarizations.

Recently, it was proposed that bursting in subicular cells results from a Ca^{2+} tail current that is activated by an action potential (Jung et al., 2001). Interestingly, these investigators found that weak- and strong-bursting phenotypes robustly correlated with the magnitude of Ca^{2+} tail currents. In agreement with these results, we found that IB^- and IB^+ cells differentially expressed TTX-resistant humps and spikes. Interestingly, at 1 mM Ca^{2+}, bursting in IB^- cells was not significantly affected, whereas burst duration in IB^+ neurons was reduced. This support the idea advanced by Jung et al. (2001) that a difference in the Ca^{2+} currents between IB^+ and IB^- cells could explain their different ability to burst.

Nevertheless, we also found evidence for a role of Na^+ currents in subicular bursting. We found that ADPs underlying bursting were blocked by high and low concentrations of TTX in both IB^+ and IB^- cells, in a similar way to the persistent Na^+-dependent ADP described in some hippocampal cells (Jensen et al., 1996; Azouz et al., 1996). Because even low concentration of TTX could affect the propagation of action potentials all along the somatodendritic axis (Mackenzie and Murphy, 1998), we also evaluated the effect of low concentrations of TTX on ADPs elicited by subthreshold current pulses, as well as the effect of local somatic application. In both cases we found that ADPs were blocked by TTX, and bursting was eliminated. Interestingly, local application of TTX into the apical dendrite did not block bursting. All these findings strongly support a role of somatic subthreshold Na^+ currents, probably through the persistent Na^+ current, on bursting in subicular cells.

However, it is known that both extracellular and intracellular Ca^{2+} can affect Na^+-persistent currents, thus shaping ADPs (Su et al., 2001). In neonatal granule cells and adult cortical cells, low-threshold Ca^{2+} currents are involved in the generation of ADPs (Zhang et al., 1993; Azouz et al., 1996; Geijo-Barrientos, 2000), thus contributing to bursting. This is in agreement with our observation that depolarizing the resting membrane potential resulted in a regular-spiking instead of a bursting pattern (Fig. 3E) (Stewart and Wong, 1993; Mason, 1993; Mattia et al., 1997). At these depolarized membrane potentials, ADPs can still be detected (Fig. 3Ea, arrow), suggesting that other high-threshold components (e.g., the persistent Na^+ currents and high-threshold Ca^{2+} currents) are participating in their generation. Actually, bursting mechanisms may be slightly different in hyperpolarization- and depolarization-induced bursting (Figs. 3Eb and 4Cb).

In summary, our data support the idea that bursting in subicular neurons results from a delicate balance between fast-Na^+ and Ca^{2+} currents, as recently suggested by Jung et al. (2001). However, our results also suggest an important role of other Na^+-dependent component in shaping ADPs, probably through persistent channels (Mattia et al., 1993, 1997). In favor of this idea are the lack of ADPs and bursting in regular-spiking cells in which Ca^{2+} humps were recorded, and the absence of bursting when ADPs were blocked by low and local concentrations of TTX. Therefore, the delicate ionic balance underlying bursting would depend on the type and spatial distribution of channels expressed in a particular cell. The two different subclasses of bursting cells, IB^- and IB^+, appear to involve different amounts of Ca^{2+} currents, which could determine their differential ability to burst in response to current pulses and orthodromic stimulation. This variability within the bursting cell group could be important when considering the ionic mechanisms underlying subicular bursting.

Subicular Regular-Spiking Cells

According to our data, regular-spiking cells were the most common electrophysiological phenotype present throughout the ventral subicular complex. They were encountered in both deep and superficial layers. Regular-spiking cells are widely present in the central nervous system (CNS). In the subiculum, regular-spiking cells were initially reported by some investigators (Stewart and Wong, 1993; Mason, 1993; Taube, 1993), but not by others (Mattia et al., 1993). Subicular regular-spiking cells, but not bursting cells, were found to show nicotinamide adenine dinucleotide phosphate-diaphorase (NADPH-d) activity (Greene et al., 1997) and a lower effect of neuropeptide somatostatin (Greene and Mason, 1996). This suggests a neurochemical separation of subicular regular-spiking cells.

We found that subicular regular-spiking cells can be subclassified into two different electrophysiological populations, RSA and

RST cells, according to the degree of firing adaptation. Morphologically, they exhibited slight differences in the width and the first bifurcation of their principal apical dendrite. Like bursting cells, regular-spiking neurons project to the CA1/alveus and within the subicular complex. Electrophysiologically, both responded with single spikes to alvear extracellular stimulation, in a similar way to IB^-, but not to IB^+ cells. RSA and RST cells shared similar properties, except for a lower input resistance in RST compared with RSA cells from the subiculum and the PrS and PaS deep layers. Interestingly, the input resistance of regular-spiking cells was similar to that found in IB^- cells, but not in IB^+ cells. This difference in input resistance between regular-spiking and bursting (IB^+) cells concurs with the findings of some studies (Greene and Totterdell, 1997), and is in contrast to those of others (Taube, 1993; Staff et al., 2000). It is therefore important to establish which subclasses of bursting and regular-spiking cells are being compared, as the statistical differences of some parameters appear to be related to particular electrophysiological subgroups. Indeed, because of the slight overlap of the adaptation indices of RSA and RST cells, it could be suggested that regular-spiking cells may constitute one group with a Gaussian distribution of the adaptation degree. However, because of input resistance of RSA and RST cells was different and because of significant differences with bursting cells were more likely to be detected when the two subgroups are considered, we suggest the electrophysiological separation of these cells.

Other Subicular Cell Types: MPO Cells and Fast-Spiking Interneurons

The remaining 20% of cells from the subicular complex were fast-spiking interneurons and unclassified cells that included neurons showing intrinsic membrane potential oscillations (MPO cells, 6%). MPO cells were encountered exclusively in the deep layers of the subiculum, PrS, and PaS areas. Interestingly, the spatial distribution of these cells appeared to increase progressively from the subiculum toward the PaS (Fig. 8B). Axonal collaterals from these cells were found to project to the alveus of CA1 and within the subicular complex. To our knowledge, this is the first report of this electrophysiological cell type in the subicular complex. Neurons with similar electrophysiological properties have been reported in deep layers of the entorhinal cortex (Gloveli et al., 2001). They are negatively immunoreactive to γ-aminobutyric acid (GABA) and project to the subiculum and the dentate gyrus. It is possible that the progressive increase of this cellular type in the PaS direction is related to its larger presence in the entorhinal cortex, where a functional role in coordinating activity of the hippocampus and other cortical structures has been suggested (Gloveli et al., 2001).

Interneurons of the subicular complex have not been studied extensively, and there are few data on their electrophysiological and morphological properties (Kawaguchi and Hama, 1987; Stewart and Wong, 1993; Greene and Totterdell, 1997). These interneurons were described as local projecting cells that have nonpyramidal somata and several dendritic processes. Electrophysiologically, they were identified as fast-spiking cells. We found that the fast-spiking phenotype correlated well with morphologically identified interneurons in our preparation. Although we observed a certain heterogeneity in the morphological and electrophysiological characteristics of interneurons (Menendez de la Prida, unpublished observations; Porter et al., 2001), their features were as previously described in the subiculum and the hippocampus (Kawaguchi and Hama, 1987; Jones and Buhl, 1993; Freund and Buzsáki, 1996; Greene and Totterdell, 1997). It is therefore likely that the fast-spiking interneurons we found throughout the subicular complex were GABAergic inhibitory cells.

Functional Significance of the Electrophysiological Diversity of the Subicular Principal Neurons

The wide electrophysiological diversity of subicular principal neurons confers considerable versatility on this structure. It is generally assumed that the output of the subicular complex is of the bursting type. However, we found that both bursting and regular-spiking subicular cells, as well as MPO cells, are projecting neurons. This versatility of the output pattern is strengthened by the fact that subicular bursting cells may change their firing pattern from bursting to regular-spiking if they are depolarized (Fig. 3a) (Stewart and Wong, 1993; Mason, 1993; Mattia et al., 1997). Also, the response of subicular bursting and regular-spiking neurons to orthodromic stimulation of the CA1 alveus input is different (Stewart and Wong, 1993; Stewart, 1997). Alvear stimulation of subicular bursting cells elicits EPSPs that are able to trigger bursts in IB^+, but not in IB^- cells, where single spikes are typically induced (Fig. 3Ga,b). This lack of orthodromically induced bursts in IB^- cells makes them similar to regular-spiking cells, where orthodromic stimulation only induced single spikes (Fig. 2Ga,b). Therefore, the electrophysiological subicular output is probably highly adaptable, with projecting neurons having both regular and bursting firing patterns that can be adjusted by subtle voltage changes.

Electrophysiological diversity is also important for the functioning of local subicular circuits, which are characterized by a simple columnar and laminar organization (Funahashi and Stewart, 1997a; Naber and Witter, 1998; Harris et al., 2001). Locally, bursting cells can act as pacemakers of network activity, as they can burst spontaneously, as shown both in vivo (Finch et al., 1988; Gigg et al., 2000) and in vitro (Harris et al., 2001). This ability endows local subicular circuits with a structural support to amplify incoming inputs (Taube et al., 1990; Sharp and Green, 1994), but bursting cells can also participate in the development of brain rhythms (Stanford et al., 1998) and pathological activity such as epilepsy (Behr and Heinemann, 1996; Harris et al., 2001). In normal conditions, the widespread presence of putative GABAergic fast-spiking interneurons provides a local inhibitory control of excitation and bursting. Nevertheless, impairment of GABAergic inhibition in the subicular complex reveals polysynaptic excitation of both bursting and regular-spiking cells, resulting in epileptiform

discharges (Funahashi et al., 1999; Harris et al., 2001; Menendez de la Prida and Pozo, 2002).

The subicular complex acts as the principal bilateral output of the hippocampal formation to different areas, such as the entorhinal cortex and other brain nuclei (Witter, 1993; Ishizuka, 2001); it and also receives reciprocal inputs from them. These afferent and efferent projecting patterns are differently distributed in the different areas of the subicular complex, i.e., the subiculum, PrS, and PaS (Köhler, 1984a; Witter, 1993; Ishizuka, 2001). In contrast to the hippocampus, the subicular complex is more poorly known, and many of its intrinsic and functional properties are matters for discussion (O'Mara et al., 2001). The electrophysiological diversity described here suggests that the subicular complex is much more complex than originally thought, and that further efforts are required in order to discover both in vitro and in vivo its properties and function.

Acknowledgments

The authors thank E. Geijo-Barrientos, M. Maravall, and A. Agmon for useful comments and suggestions. E.D. Martín provided useful comments and suggestions on a draft of this article. We also thank J. DeFelipe for helping us with the morphological classification of neurons and J. Arellano for discussions on the cytoarchitectonic organization of the subicular complex.

REFERENCES

Agmon A, Connors BW. 1989. Repetitive burst-firing neurons in the deep layers of mouse somatosensory cortex. Neurosci Lett 99:137–141.

Alonso A, Llinas RR. 1989. Subthreshold Na^+-dependent theta-like rhythmicity in stellate cells of entorhinal cortex layer. II. Nature 342: 175–177.

Azouz R, Jensen MS, Yaari Y. 1996. Ionic basis of spike after-depolarization and burst generation in adult rat hippocampal CA1 pyramidal cells. J Physiol 492.1:211–223.

Bal T, McCormick DA. 1993. Mechanisms of oscillatory activity in guinea-pig nucleus reticularis thalami in vitro: a mammalian pacemaker. J Physiol 468:669–691.

Behr J, Heinemann U. 1996. Low Mg^{2+} induced epileptiform activity in the subiculum before and after disconnection from rat hippocampal and entorhinal cortex slices. Neurosci Lett 205:25–28.

Behr J, Empson RM, Schmitz D, Gloveli T, Heinemann U. 1996. Electrophysiological properties of rat subicular neurons in vitro. Neurosci Lett 220:41–44.

Davies DC, Wilmott AC, Mann DM. 1988. Senile plaques are concentrated in the subicular region of the hippocampal formation in Alzheimer's disease. Neurosci Lett 94:228–233.

Finch DM, Tan AM, Isokawa-Akesson M. 1988. Feedforward inhibition of the rat entorhinal cortex and subicular complex. J Neurosci 8:2213–2226.

Flood DG. 1991. Region-specific stability of dendritic extent in normal human aging and regression in Alzheimer's disease. II. Subiculum. Brain Res 540:83–95.

Freund T, Buzsáki G. 1996. Interneurons of the hippocampus. Hippocampus 6:197–205.

Funahashi M, Stewart M. 1997a. Presubicular and parasubicular cortical neurons of the rat: functional separation of deep and superficial neurons in vitro. J Physiol 501.2:387–403.

Funahashi M, Stewart M. 1997b. Presubicular and parasubicular cortical neurons of the rat: electrophysiological and morphological properties. Hippocampus 7:117–129.

Funahashi M, Harris E, Stewart M. 1999. Re-entrant activity in a presubiculum-subiculum circuit generates epileptiform activity in vitro. Brain Res 849:139–146.

Geijo-Barrientos E. 2000. Subthreshold inward membrane currents in guinea-pig frontal cortex neurons. Neuroscience 95:965–972.

Gigg J, Finch DM, O'Mara SM. 2000. Responses of rat subicular neurons to convergent stimulation of lateral entorhinal cortex and CA1 in vivo. Brain Res 884:35–50.

Gloveli T, Dugladze T, Schimitz D, Heinemann U. 2001. Properties of entorhinal cortex deep layer neurons projecting to the rat dentate gyrus. Eur J Neurosci 13:413–420.

Gray JA, Feldon J, Rawlins JNP, Hemsley DR, Smith AD. 1991. The neuropsychology of schizophrenia. Behav Brain Sci 14:1–84.

Greene JRT. 1996. The subiculum: a potential site of action for novel antipsychotic drugs? Mol Psychiatry 1:380–387.

Greene JRT, Mason A. 1996. Neuronal diversity in the subiculum: correlation with the effects of somatostatin on intrinsic properties and on GABA-mediated IPSPs in vitro. J Neurophysiol 76:1657–1666.

Greene JRT, Totterdell S. 1997. Morphology and distribution of electrophysiologically defined classes of pyramidal and nonpyramidal neurons in rat ventral subiculum in vitro. J Comp Neurol 380:395–408.

Greene JRT, Lin H, Mason AJR, Johnson LR, Totterdell S. 1997. Differential expression of NADPH-diaphorase between electrophysiologically-defined classes of pyramidal neurons in rat ventral subiculum, in vitro. Neuroscience 80:95–104.

Halliwell JV, Adams PR. 1982. Voltage-clamp analysis of muscarinic excitation in hippocampal neurons. Brain Res 250:71–92.

Harris E, Stewart M. 2001. Intrinsic connectivity of the rat subiculum. II. Properties of synchronous spontaneous activity and a demonstration of multiple generator regions. J Comp Neurol 436:506–518.

Harris E, Witte MP, Weinstein G, Stewart M. 2001. Intrinsic connectivity of the rat subiculum. I. Dendritic morphology and patterns of axonal arborization by pyramidal neurons. J Comp Neurol 436:490–505.

Ishizuka N. 2001. Laminar organization of the pyramidal cell layer of the subiculum in the rat. J Comp Neurol 435:89–110.

Jensen MS, Azouz R, Yaari Y. 1996. Spike after-depolarization and burst generation in adult rat hippocampal CA1 pyramidal cells. J Physiol 492.1:199–210.

Jones RSG, Buhl EH. 1993. Basket-like interneurons in layer II of the entorhinal cortex exhibit a powerful NMDA-mediated synaptic excitation. Neurosci Lett 149:35–39.

Jung H, Staff NP, Spruston N. 2001. Action potential bursting in subicular pyramidal neurons is driven by a calcium tail current. J Neurosci 21:3312–3321.

Kawaguchi Y. 1995. Physiological subgroups of nonpyramidal cells with specific morphological characteristics in layer II/III of rat frontal cortex. J Neurosci 15:2638–2655.

Kawaguchi Y, Hama K. 1987. Fast-spiking non-pyramidal cells in the hippocampal CA3 region, dentate gyrus and subiculum of rats. Brain Res 425:351–355.

Köhler C. 1986a. Intrinsic projections of the retrohippocampal region in the rat brain. I. The subicular complex. J Comp Neurol 236:504–522.

Köhler C. 1986b. Intrinsic projections of the retrohippocampal region in the rat brain. II. The medial entorhinal cortex. J Comp Neurol 246: 149–169.

Mackenzie PJ, Murphy TH. 1998. High safety factor for action potential conduction along axons but not dendrites of cultured hippocampal and cortical neurons. J Neurophysiol 80:2089–2101.

Magee JC, Carruth M. 1999. Dendritic voltage-gated ion channels regulate the action potential firing mode of hippocampal CA1 pyramidal neurons. J Neurophysiol 82:1895–1901.

Mason A. 1993. Electrophysiology and burst-firing of rat subicular pyramidal neurons in vitro: a comparison with area CA1. Brain Res 600: 174–178.

Mattia D, Hwa GGC, Avoli M. 1993. Membrane properties of rat subicular neurons in vitro. J Neurophysiol 70:1244–1248.

Mattia D, Kawasaki H, Avoli M. 1997. In vitro electrophysiology of rat subicular bursting neurons. Hippocampus 7:48–57.

Menendez de la Prida L, Suarez F, Pozo MA. 2002. The effect of different morphological sampling criteria on the fraction of bursting cells recorded in the rat subiculum in vitro. Neurosci Lett 322:49–52.

Menendez de la Prida L, Pozo MA. 2002. Excitatory and inhibitory control of epileptiform discharges in combined hippocampal/entorhinal cortical slices. Brain Res 940:27–35.

Naber PA, Witter MP. 1998. Subicular efferents are organized mostly as parallel projections: a double-labeling, retrograde-tracing study in the rat. J Comp Neurol 393:284–297.

O'Mara SM, Commins S, Anderson M, Gigg J. 2001. The subiculum: a review of form, physiology and function. Prog Neurobiol 64:129–155.

Paxinos G, Watson C. 1986. The rat brain in stereotaxic coordinates. 2nd ed. San Diego, CA: Academic Press.

Porter JT, Johnson CK, Agmon A. 2001. Diverse types of interneurons generate thalamus-evoked feedforward inhibition in the mouse barrel cortex. J Neurosci 21:2699–2710.

Rall W. 1969. Time constants and electrotonic length of membrane cylinders and neurons. Biophys J 9:1483–1508.

Sharp PE, Green C. 1994. Spatial correlates of firing patterns of single cells in the subiculum of freely moving rat. J Neurosci 14:2339–2356.

Stanford IM, Traub RD, Jefferys JGR. 1998. Limbic gamma rhythms. II. Synaptic and intrinsic mechanisms underlying spike doublets in oscillating subicular neurons. J Neurophysiol 80:162–171.

Staff NP, Jung H, Thiagarajan T, Yao M, Spruston N. 2000. Resting and active properties of pyramidal neurons in subiculum and CA1 of rat hippocampus. J Neurophysiol 84:2398–2400.

Stewart M. 1997. Antidromic and orthodromic responses by subicular neurons in rat brain slices. Brain Res 769:71–85.

Stewart M, Wong RK. 1993. Intrinsic properties and evoked responses of guinea-pig subicular neurons in vitro. J Neurophysiol 70:232–245.

Su H, Alroy G, Kirson ED, Yaari Y. 2001. Extracellular calcium modulates persistent sodium current-dependent burst-firing in hippocampal pyramidal neurons. J Neurosci 21:4173–4182.

Taube JS. 1993. Electrophysiological properties of neurons in the rat subiculum in vivo. Exp Brain Res 96:304–318.

Taube JS, Muller RU, Ranck JB Jr. 1990. Head-direction cells recorded from the postsubiculum in freely moving rats. I. Description and quantitative analysis. J Neurosci 10:420–435.

Traub RD, Jefferys JGR, Miles R, Whittington MA, Toth K. 1994. A branching dendritic model of a rodent CA3 pyramidal neuron. J Physiol 481:79–95.

Van Groen T, Lopes da Silva FH. 1986. Organization of the reciprocal connections between the subiculum and the entorhinal cortex in the cat. II. An electrophysiology study. J Comp Neurol 251:111–120.

Witter MP. 1993. Organization of the entorhinal-hippocampal system: a review of current anatomical data. Hippocampus 3:33–44.

Zhang L, Valiante TA, Carlen PL. 1993. Contribution of the low-threshold T-type calcium current in generating the post-spike depolarization afterpotential in dentate granule neurons of immature rats. J Neurophysiol 70:223–231.